HHS Public Access

Author manuscript

Cancer Immunol Res. Author manuscript; available in PMC 2023 January 01.

Published in final edited form as:

Cancer Immunol Res. 2022 July 01; 10(7): 871–884. doi:10.1158/2326-6066.CIR-21-0691.

P2RX7 enhances tumor control by CD8+ T cells in adoptive cell therapy

Kelsey M. Wanhainen[1], **Changwei Peng**[1], **Maggie H. Zhou**[3], **Bruna de Gois Macedo**[3], **Stephen O'Flanagan**[2], **Tingyuan Yang**[1], **Ameeta Kelekar**[1], **Brandon J. Burbach**[1], **Henrique Borges da Silva**[1,3], **Stephen C. Jameson**[1]

[1]University of Minnesota Center for Immunology, Masonic Cancer Center, Department of Laboratory Medicine and Pathology, Minneapolis MN

[2]Department of Microbiology and Immunology, Minneapolis MN

[3]Mayo Clinic, Department of Immunology, Scottsdale, AZ

Abstract

Expression of the purinergic receptor P2RX7 by $CD8^+$ T cells promotes generation of memory populations following acute infections. However, data suggest that P2RX7 may limit the efficacy of antitumor responses. Herein, we show that P2RX7 is beneficial for optimal melanoma control in a mouse $CD8^+$ T cell adoptive transfer model. Tumor specific *P2rx7*$^{-/-}$ $CD8^+$ T cells exhibited impaired mitochondrial maintenance and function but did not display signs of overt exhaustion early in the antitumor response. However, as the tumor burden increased, the relative frequency of P2RX7-deficient $CD8^+$ T cells declined within the tumor; this correlated with reduced proliferation, increased apoptosis and mitochondrial dysfunction. Extending these studies, we found that transient *in vitro* stimulation of P2RX7 using the ATP analog BzATP led to enhanced B16 melanoma control by $CD8^+$ T cells. These findings are in keeping with the concept that extracellular ATP (eATP) sensing by P2RX7 on $CD8^+$ T cells is required for their ability to efficiently eliminate tumors by promoting mitochondrial fitness and underscore the potential for P2RX7 stimulation as a novel therapeutic treatment to enhance tumor immunotherapy.

Keywords

Immunotherapy; P2RX7; $CD8^+$ T-cell metabolism; B16 melanoma; eATP

Introduction

The purinergic receptor P2RX7 is a ligand-gated ion channel that recognizes extracellular ATP (eATP) [1]. P2RX7 stimulation induces Ca^{2+} influx and K^+ efflux, but prolonged exposure to very high eATP concentrations results in the formation of a macropore that

Address correspondence to: Stephen C. Jameson, University of Minnesota Medical School, 2-184 WMBB, 2101 6th St SE, Minneapolis MN 55455; james024@umn.edu, phone number: 612-625-1496 or Henrique Borges da Silva, Mayo Clinic, 13400 E. Shea Boulevard, Samuel C. Johnson Building 3-364, Scottsdale, AZ 85259; BorgesdaSilva.Henrique@mayo.edu, phone number: 480-301-3592.

Disclosures: The authors declare no potential conflicts of interest

ultimately induces cell death [1, 2]. Elevated concentrations of eATP can act as a “danger signal” during infection or acute tissue damage, but eATP also accumulates in many solid tumors and is a component of the tumor microenvironment (TME) [3]. In myeloid cells, P2RX7 stimulation leads to assembly of the NLPR3 inflammasome and promotes immunogenic cell death, innate immune activation, and enhanced presentation of tumor antigens [4]. Accordingly, previous studies have shown that host deficiency of P2RX7 leads to accelerated growth of B16 melanoma tumors, which is accompanied by reduced lymphocyte infiltration and decreased intratumoral inflammatory cytokines [5, 6]. As a result of these studies, P2RX7 is thought to promote antitumor immune responses. However, some tumors express conformationally altered forms of P2RX7 that may promote their survival in the eATP-rich TME, while P2RX7 expressed by tumor-infiltrating immune cells makes them vulnerable to macropore formation and death [7]. Hence the impact of P2RX7 on tumor growth and control is complex.

P2RX7 is also expressed by numerous T-cell populations and is important for metabolic fitness and durability of memory $CD8^+$ T cells following acute and chronic infections [8, 9]. Parallels between $CD8^+$ T-cell responses in chronic infections and tumors suggests that P2RX7 may have a similarly beneficial role in $CD8^+$ T cell–mediated antitumor immunity. On the other hand, it has been proposed that the abnormally high eATP concentrations in the TME could instead result in P2RX7-mediated T-cell death [7]. Indeed, using an adoptive cell therapy (ACT) approach, one study suggests that P2RX7 expression by mouse $CD8^+$ T cells limits their ability to control the growth of B16 melanoma [10]. However, that study employed $CD8^+$ T cells that were expanded with IL2 alone, and it is known that inclusion of IL12 during $CD8^+$ T-cell stimulation substantially improves tumor control in B16 melanoma models, mediated through increased production of $CD8^+$ effector cytokines and decreased induction of inhibitory receptors associated of T-cell exhaustion [11, 12]. Hence, it is unclear whether P2RX7 limits or enhances the immunotherapeutic potential of ACT using optimally activated $CD8^+$ T cells.

T cell–based immunotherapies have already led to impressive outcomes in the clinic for patients with a variety of malignancies [13–15]. However, there are still barriers hindering these therapies from reaching their full potential, and a pressing need to better understand how the TME impairs T-cell accumulation, function, and survival. Determining whether expression and stimulation of P2RX7 on tumor-specific $CD8^+$ T cells is an asset or detriment for tumor immunotherapy is important to inform strategies that could enhance the efficacy and durability of T cell ACTs. In is becoming clear that mitochondrial function is compromised in tumor-infiltrating T cells, and that strategies that enhance the levels of functional mitochondria improve ACT by $CD8^+$ T cells [16–20]. Our previous work shows that P2RX7 signaling in long-lived memory $CD8^+$ T-cell subsets is essential for normal mitochondrial homeostasis and function, with P2RX7-deficiency leading to impaired mitochondrial maintenance, function, and ultrastructure; dysregulated oxidative phosphorylation (OXPHOS); and altered levels of intracellular ATP and AMP [8, 9]. However, there is evidence that the different levels of P2RX7 stimulation may enhance or inhibit mitochondrial maintenance [1, 21], so it is currently unclear how the presence of P2RX7 impacts mitochondrial function and T-cell survival in the eATP-rich TME of solid tumors [7].

In this study, we demonstrate a $CD8^+$ T cell–intrinsic role for P2RX7 in promoting antitumor immune responses, using the B16 melanoma model. This effect was observed for $CD8^+$ T cells activated in the presence of IL12, which substantially enhances tumor control and simultaneously leads to increased P2RX7 expression. P2RX7-deficiency resulted in impaired mitochondrial homeostasis of transferred $CD8^+$ T cells, in keeping with previous studies [8, 9]. Furthermore, *P2rx7*$^{-/-}$ $CD8^+$ T cells displayed elevated expression of certain exhaustion markers, increased apoptosis, reduced proliferation, and selective loss as the tumor burden increased. Additionally, we found that transient *in vitro* stimulation of $CD8^+$ T cells with a P2RX7 agonist in place of IL12 also improved ACT and enhanced mitochondrial function while reducing expression of some exhaustion markers. These results indicate that P2RX7 expression and stimulation can be leveraged to promote optimal $CD8^+$ T cell–mediated antitumor immunity.

Materials and Methods

Supplementary Table S1 provides information on the reagents used in this study, including RRID.

Mice

Female 6- to 8-week-old adult C57BL/6 and B6.SJL mice were purchased from Charles River (via the National Cancer Institute). *P2rx7*$^{-/-}$ mice were purchased from Jackson Laboratories and backcrossed to the P14 (LCMV-gp33/D^b specific) and OT-I (OVA/K^b specific) TCR transgenic backgrounds, provided by R. Ahmed (Emory University) and K. Hogquist (University of Minnesota), respectively. Thy-1 and CD45 were introduced as congenic markers to distinguish wild-type (WT) and *P2rx7*$^{-/-}$ cells using B6.SJL (CD45.1) or B6.PL (Thy1.1) mice purchased from either Charles River or Jackson Laboratories. Animals were maintained under specific-pathogen-free conditions at the University of Minnesota. All experimental procedures were approved by the Institutional Animal Care and Use Committee at the University of Minnesota. Animals were randomly assigned to experimental groups.

Cell lines

B16.gp33 cells (provided by Dr. Ananda Goldrath, University of California, San Diego, in 2018) and B16.OVA cells (provided by Dr. Matt Mescher, University of Minnesota, in 2003) were cultured in RPMI 1640 (Corning, #10-040-CV) supplemented with 10% FBS (Atlas Biologicals, #FS-0500-AD), 100 U/mL penicillin/streptomycin (Gibco, #15070063), and 2mM L-glutamine (Corning, #25-005-CI). After thawing cell lines, B16 cells were expanded for 3 days and passaged once prior to transfer into mice. Cell lines did not undergo Mycoplasma testing. Authentication of OVA or gp33 expression on tumor cell lines was confirmed by *in vitro* or *in vivo* recognition by OT-I or P14 $CD8^+$ T-cells, respectively.

In vitro activation and adoptive transfer of $CD8^+$ T cells

Naïve $CD8^+$ T cells were isolated from the spleens of WT or *P2rx7*$^{-/-}$ P14 or OT-I transgenic mice with the mouse naïve $CD8^+$ T cell isolation kit (Miltenyi Biotech, #130-096-543). A total of 2.5×10^5 isolated T cells were stimulated in flat bottom 24-

well plates with anti-CD3 (10 ug/mL) (BioXCell, #BE0001-1), anti-CD28 (20 ug/mL) (BioXCell, #BE0015-1), human IL2 (2.5 IU/mL) (Peprotech, #200-02), and with or without murine IL12 (5 ng/mL) (R&D Systems #419-ML-050/CF) for 72 hours in RPMI 1640 medium supplemented with 10% FBS, 100 U/mL penicillin/streptomycin, 2mM L-glutamine at 37°C/5% CO_2. For P2RX7 agonism experiments, isolated $CD8^+$ T cells were similarly activated with anti-CD3/-CD28 and IL2, then 100μM of BzATP (Sigma Aldrich, #B6396-25MG), or dH_2O as a vehicle treatment, was added every 24 hours to the cultures for the 72-hour activation. After 72 hours, $2.5 \times 10^5 – 5.0 \times 10^5$ activated T cells were transferred intravenously (i.v.) into recipient mice (see In vivo tumor experiments).

In vivo tumor experiments

Mice were injected subcutaneously with $1.5 \times 10^5 – 3.0 \times 10^5$ B16.gp33 cells or B16.OVA cells in the right flank. After tumors became palpable (~7 days), tumor-bearing mice received 5.0×10^5 activated P14 or OT-I T cells (or 2.5×10^5 of each for co-transfer experiments). Tumor growth and survival was monitored by measuring height and width every other day with calipers until mice reached an end-point criteria of $100mm^2$ or ulceration. Where indicated in the figure legends, mice were treated with a P2RX7 antagonist A-438079 (80mg/kg) (Abcam #ab120413), or PBS as a vehicle treatment, intraperitoneally (i.p.) every other day beginning when tumors became palpable (~7 days post tumor injection).

Flow cytometry

Mice were sacrificed at times indicated in the figure legends and spleens, tumor-draining inguinal lymph nodes (dLN) and tumors were harvested and homogenized. In all experiments involving isolation of lymphocytes from tumors, 50μg of Treg-Protector (anti-ARTC2.2) nanobody (BioLegend #149802) was injected intravenously (i.v.) 30 minutes prior to mouse sacrifice as previously described [8, 9]. Tumors were removed, cut into small pieces, and digested with 3mg/mL Collagenase type I (Worthington #LS004197) solution for 1 hour at 37°C and then dissociated via gentleMACS Dissociator (Miltenyi Biotec) twice. Spleens and dLNs were homogenized and passed through a 70um cell strainer. Isolated mouse cells were stained with antibodies specific for CD8α (clone 53–6.7, BD Biosciences), CD44 (clone IM7, Tonbo Biosciences), CD69 (clone H1.2F3, BioLegend), CD103 (clone M290, BD Biosciences), P2RX7 (clone 1F11, BD Biosciences), CD279 (PD-1) (clone 29F.1A12, Biolegend), CD366 (Tim3) (clone RMT3-23, BioLegend), CD223 (Lag3) (clone C9B7W, BioLegend), CD39 (clone Duha59, Biolegend), TCF1 (clone C63D9, Cell Signaling Technologies), TOX (clone TXRX10, Thermo), Ki67 (clone SolA15, Thermo), IFNγ (clone XMG1.2, Tonbo Biosciences), granzyme B (clone GB11, Thermo Fisher Scientific). All cells were stained at antibody dilutions of 1:200, except for granzyme B (1:100), IFNγ (1:100), TCF1 (1:100), TOX (1:50), and P2RX7 (1:50). Cells stained intracellularly for granzyme B, IFNγ, Ki67, TCF1, and Tox were permeabilized using the FoxP3/Transcription Factor fixation/permeabilization kits (Tonbo Biosciences #TNB-0607-KIT) according to the manufacturer's protocols. Cell viability was determined with Ghost Dye 780 (Tonbo Biosciences #13-0865-T100). Enumeration of lymphocytes was achieved using CountBright Absolute Counting Beads (Invitrogen #C36950).

For *ex vivo* restimulation assays, digested/homogenized tumors, dLNs and spleens were incubated with 2ul/mL PMA/Ionomycin cell stimulation cocktail (Tonbo Biosciences #TNB-4975-UL400) for 4 hours at 37°C in RPMI 1640 supplemented with 2% FBS. We then proceeded with extracellular/intracellular staining as described above.

For mitochondrial mass and membrane potential measurements, 1–2×10^6 cells were incubated with 100nM MitoTracker Green (MTG) (Thermofisher Scientific #M7514) and 80nM Tetramethylrhodamine ethyl ester (TMRE) (Thermo Fisher Scientific #T669) simultaneously for 20 minutes in RPMI 1640 supplemented with 2% FBS at 37°C prior to *ex vivo* staining. In order to account for experiment-to-experiment variability, geometric mean fluorescence intensities (gMFIs) of either MTG or TMRE in donor WT $CD8^+$ P14 cells within the spleen of each experiment were averaged and fold change of donor WT or *P2rx7*$^{-/-}$ $CD8^+$ T cells within the tumor or tumor dLN for each experiment was calculated relative to splenic WT donor cells. Mitochondrial reactive oxygen species (ROS) were evaluated by incubating 1–2×10^6 cells with 5μM MitoSOX reagent (ThermoFisher #M36008) in RPMI 1640 supplemented with 2% FBS at 37°C prior to *ex vivo* staining.

Apoptosis was analyzed using an Annexin V Apoptosis Detection Kit I (BD #556454) according to manufacturer's instructions. Briefly, after extracellular staining, cells were washed 2x in PBS (without serum) and resuspended in Annexin V binding buffer. Approximately 15–30 minutes prior to reading the samples, Annexin V-APC and Propidium Iodide (PI) staining solution was added directly to the sample in Annexin V binding buffer. Apoptotic cells were discriminated from dead/necrotic cells by PI and viability ghost dye staining (i.e., Annexin V^+ LD/PI^-).

Flow cytometric analysis was performed on a LSR II or LSR Fortessa (BD Biosciences) and data was analyzed using FlowJo software v10.8 (Treestar).

Metabolic assays

Oxygen consumption rate (OCR) and extracellular acidification rate (ECAR) were assessed in *in vitro* activated WT and *P2rx7*$^{-/-}$ T cells (activated with or without IL12 or BzATP for 72 hours) using a 96-well XF Extracellular flux analyzer, according to the manufacturer's instructions (Seahorse Bioscience), similar to earlier studies [8, 9]. Briefly, 2×10^5 activated cells were plated onto Seahorse XFe96 (Agilent) plates coated with CellTak (Corning 354240) solution the night before in warm Seahorse base media (Agilent #102353-100) supplemented with 2mM L-glutamine, 1mM sodium pyruvate (Corning #25-000-Cl), and 10mM glucose (Sigma G8769-100ML) (pH 7.4) the day of assay. Seahorse XF Mito Stress kit (Agilent #103015-100) components (1.5μM Oligomycin, 1μM FCCP, 0.5μM Rotenone/AntimycinA) were added to hydrated 96-well sensor cartridge (incubated overnight at 37°C with Agilent calibrant solution) before performing the assay. Spare respiratory capacity (SRC) and OCR and ECAR values were defined as previously described [16, 22].

Tumor-killing assay

Killing of B16 melanoma cells was evaluated in real-time using the IncuCyte platform. Activated WT or *P2rx7*$^{-/-}$ P14 $CD8^+$ T cells were plated into 96-well flat clear-bottom tissue culture–treated microplates, previously coated with Poly-L-ornithine (Sigma Aldrich

#A-004-M) for 2–3 hours, along with CellTrace Far Red (Thermo Fisher Scientific #C34564) stained (according to manufacturer's instructions) B16.gp33 or B16.OVA cells at 1:1 and 3:1 effector:target ratios. 5uM of Caspase-3/7 green dye (Sartorius #4440) was added just prior to beginning assay to identify dying cells. The plate was then placed in an IncuCyte ZOOM platform housed inside a cell incubator at 37°C/5% CO_2. Images from 5 technical replicates were taken every 30 minutes for 48 hours using a 4X objective lens and then analyzed using IncuCyte Basic Software v2018A (Sartorius). Graphed readouts represent percentage of live B16 melanoma targets (CellTrace Far $Red^+Caspase\text{-}3/7^-$), normalized to live targets alone at the starting (0 hour) time point.

Human $CD8^+$ T-cell cultures

Resting $CD8^+$ T cells were isolated from Ficoll-purified PBMC isolates from leukapheresis products (Memorial Blood Center, St. Paul, MN) using a naïve human $CD8^+$ negative selection kit (Stem Cell #19258). Purified cells were stimulated for 72 hours with anti-CD3/-CD28beads (Gibco #11161D) with 4ng/mL human IL2, and with or without 50ng/mL IL12 (R&D systems #219-IL-005/CF). After 72 hours, activated $CD8^+$ T cells continued to be cultured with concentrations of IL2 +/− IL12 indicated in the figure legends until RNA expression analysis.

RNA expression analysis

Human $CD8^+$ T cells activated with IL2 +/− IL12 were first homogenized using QIAshredder columns (QIAGEN) and RNA was extracted using RNeasy kit (QIAGEN #79654) following the manufacturer's instructions. From isolated RNA samples, cDNA was prepared with the SuperScript III First-Strand Synthesis SuperMix (ThermoFisher Scientific #11752050) following manufacturers' instructions. Gene expression was assessed (in triplicate) with an ABI 7700 sequence-detection system, and amplification was detected with SYBR Green PCR Master Mix (Applied Biosystems #4309155) as previously described [23]. The sequences of primer pairs used to measure *P2RX7* RNA were: forward, 5'- TGT GTC CCG AGT ATC CCA CC −3', reverse, 5'- GGC ACT GTT CAA GAG AGC AG −3'; the primers for glucuronidase beta (*GUSB*) (used as a control housekeeping gene) [24] were: forward, 5'- GTC TGC GGC ATT TTG TCG −3', reverse, 5'- CAC ACG ATG GCA TAG GAA TGG −3'.

Statistical analysis

Data were subject to Kolmogorov-Smirnov test to assess normality of samples. Statistical differences were calculated by using paired or unpaired two-tailed Student's t-test or one-way ANOVA with Tukey post-test. In cases where one group in the comparisons was normalized, statistical analysis employed ANOVA with Brown-Forsythe and Welch corrections. Statistical differences for survival data were assessed using a log-rank Mantel–Cox test. All statistical analysis was performed using Prism 9 (GraphPad Software). Graphical data shown with error bars indicating the SD or SEM. P values of <0.05 (*), <0.01 (**), <0.001 (***), or <0.0001 (****) indicate significant differences between groups.

Data and material availability statement

The data generated in this study are available within the article and its supplementary data files orupon request from the corresponding author Stephen C. Jameson (james024@umn.edu).

Results

P2RX7 deficiency compromises optimal CD8+ T cell ACT in melanoma.

Previous studies suggested that P2RX7 expression is necessary for the host to elicit an effective antitumor immune response [5, 6]. In striking contrast, however, one report has indicated that P2RX7-deficient CD8$^+$ T cells exhibit enhanced tumor control [10]. To investigate this further, we adoptively transferred either WT or *P2rx7*$^{-/-}$ tumor-specific transgenic CD8$^+$ T cells into mice with B16 melanoma tumors (the model used by Romagnani et al. [10]). Briefly, B16 melanoma cells expressing gp33 (B16.gp33), the epitope recognized by P14 CD8$^+$ T cells, were injected subcutaneously into WT hosts. Once tumors became palpable, either WT or *P2rx7*$^{-/-}$ P14 CD8$^+$ T cells were administered i.v. after 72 hours of *in vitro* activation (Fig. 1a). WT and *P2rx7*$^{-/-}$ P14 were activated with IL12 as a tertiary signal (in addition to anti-CD3/CD28 and IL2) to optimize antitumor immune responses, as previously described [11, 12]. Survival of tumor-bearing mice was significantly improved by adoptive transfer of WT P14 cells, compared to transfer of *P2rx7*$^{-/-}$ P14 cells (Fig. 1b). Tumor burden was also substantially reduced in mice that received WT P14 cells, with some mice having fully controlled tumors for >40 days (lines indicated by # in Fig. 1c, Supplementary Fig. S1a). In contrast, tumor control was markedly impaired in mice transferred with *P2rx7*$^{-/-}$ P14 cells (Fig. 1b–c). The effect of P2RX7 deficiency was confirmed using OT-I CD8$^+$ T cells, which were transferred into mice with B16 tumors that express ovalbumin (B16.OVA) (Fig. S1b), paralleling the system used by Romagnani et al. [10]. Despite these differences in tumor control between WT and *P2rx7*$^{-/-}$ P14 cells, there was no difference in the ability of the *in vitro* activated populations to produce IFNγ (Supplementary Fig. S1c) or kill B16 target cell lines (Supplementary Fig. S1d), in keeping with previous studies indicating that *P2rx7*$^{-/-}$ CD8$^+$ T cells differentiate normally into effector cells [8, 9].

A potentially important difference between our studies and those of Romagnani *et al.* [10] was their omission of IL12 in the CD8$^+$ T-cell activation protocol. Indeed, in parallel studies we found that the advantage we observed for WT P14 cells in controlling tumors (Fig. 1b,c) was lost if IL12 was not included during CD8$^+$ T-cell stimulation, with transfer of either WT or *P2rx7*$^{-/-}$ P14 cells only modestly improving survival of tumor-bearing mice compared to mice that received no CD8$^+$ T-cell transfer (Fig. 1d, Supplementary Fig. S2a,b). Similar outcomes were observed in the OT-I/B16-OVA model (Supplementary Fig. S2c) Consistent with Romagnani *et al.* [10], *P2rx7*$^{-/-}$ P14 cells stimulated without IL12 conferred slightly improved survival relative to WT P14 cells (Fig. 1d), although this was not statistically significant in our hands. IL12 exposure has been reported to increase P2RX7 expression on CD8$^+$ T cells [25], and we confirmed this on P14 cells assessed at the end of *in vitro* activation (Supplementary Fig. S2d). Similarly, *P2RX7* gene expression by human CD8$^+$ T cells was enhanced by culture with IL12 (Supplementary Fig. S2e). This is consistent with

the hypothesis that the P2RX7-mediated contribution to tumor control may be amplified by IL12-induced expression of P2RX7.

P2rx7$^{-/-}$ CD8^{+} T cells exhibit numeric and phenotypic differences compared to WT CD8^{+} T cells.

To determine how P2RX7 deficiency impacts donor CD8^{+} T cells transferred into tumor-bearing mice, we harvested B16.gp33 tumors, dLNs, and spleens from mice 7 days post-transfer of IL12-activated WT or *P2rx7*$^{-/-}$ P14 cells. At this time point, tumor burden was only slightly greater in mice that received *P2rx7*$^{-/-}$ P14 cells as compared to recipients of WT P14 cells (Supplementary Fig. S3a), providing an opportunity to identify phenotypic differences between WT and *P2rx7*$^{-/-}$ P14 cells, which may correspond with the failure of *P2rx7*$^{-/-}$ P14 cells to effectively control tumors. This analysis revealed fewer *P2rx7*$^{-/-}$ P14 cells per gram of tumor and in the dLN and spleen, compared with WT P14 cells (Fig. 2a), despite no significant differences in the percentage of total tumor-infiltrating CD8^{+} T cells (Supplementary Fig. S3b). Although tumor control by *P2rx7*$^{-/-}$ CD8^{+} T cells was impaired, WT and *P2rx7*$^{-/-}$ P14 cells did not differ significantly in the expression of exhaustion markers Tim3 and PD-1 within the tumor. However, in the dLN, the frequency of Tim3-expressing cells and PD-1 expression levels were elevated on the *P2rx7*$^{-/-}$ P14 population relative to WT P14 cells (Fig 2b,c, Supplementary S3d,e). This finding is important in light of studies showing that cells in the dLN may constitute a reservoir for sustaining the population of antigen-specific CD8^{+} tumor-infiltrating lymphocytes [26–28]. Elevated expression of exhaustion markers may suggest recent antigen encounter or, perhaps, approaching T-cell dysfunction/exhaustion.

We found that *P2rx7*$^{-/-}$ P14 cells within the dLN exhibit effector T-cell qualities, as evidenced by an increased frequency of cell expressing granzyme B (GzmB), despite no difference in GzmB expression among the cells within the tumor (Fig. 2d). Moreover, tumor-infiltrating *P2rx7*$^{-/-}$ P14 cells were functional, efficiently producing IFNγ after *ex vivo* restimulation with PMA/Ionomycin (Supplementary Fig. S3c). Together, these data suggest that the *P2rx7*$^{-/-}$ P14 cells within the tumor are slightly reduced in number but do not show overt signs of exhaustion. However, *P2rx7*$^{-/-}$ P14 cells within the dLN, which presumably continue to seed the tumor over time, exhibit effector-like characteristics but are beginning to increase expression of markers associated with T-cell dysfunction, which may ultimately compromise the ability of *P2rx7*$^{-/-}$ P14 cells to sustain an effective antitumor response.

Tumor infiltrating *P2rx7*$^{-/-}$ CD8^{+} T cells show signs of mitochondrial dysfunction.

We have previously shown that *P2rx7*$^{-/-}$ CD8^{+} T cells have dysregulated metabolism in an acute infection model [8]. Given the correlation between T-cell metabolic fitness and efficacy of antitumor responses [29], we were interested in whether *P2rx7*$^{-/-}$ P14 cells have altered mitochondrial dynamics in response to metabolic stressors in the TME. We measured mitochondrial mass and membrane potential of WT and *P2rx7*$^{-/-}$ P14 cells from spleens, dLNs and tumors of B16.gp33-engrafted mice by staining for MTG and TMRE, respectively (Fig. 3a–c). The TMRE/MTG ratio, indicating mitochondrial activity efficiency, was decreased in *P2rx7*$^{-/-}$ P14 cells within the tumor, dLN and spleen, relative to WT

P14 cells (Fig. 3c). This suggests that, despite both WT and *P2rx7*$^{-/-}$ P14 cells increasing mitochondrial mass in response to cues in the TME, the mitochondria in tumor-infiltrating WT P14 cells are more functional than the mitochondria in tumor-infiltrating *P2rx7*$^{-/-}$ P14 cells.

Additionally, we observed a population of P14 cells that had increased mitochondrial mass (MTG^{hi}) but very low mitochondrial membrane potential (TMRE^{lo}) (Fig. 3d). This population (MTG^{hi}TMRE^{lo}) likely represents cells that accumulate 'depolarized' and nonfunctional mitochondria, and this is known to occur at a higher frequency among CD8^{+} T cells within the TME [19]. Consistent with this, we found that both WT and *P2rx7*$^{-/-}$ P14 cells from tumors of some B16.gp33 engrafted mice had a higher percentage of MTG^{hi}TMRE^{lo} cells compared to P14 cells from the dLNs and spleens. Despite high variability among samples, this trended higher for tumor-infiltrating *P2rx7*$^{-/-}$ P14 cells compared to WT (Fig. 3d). Together, these results suggest that tumor-infiltrating P14 cells that lack P2RX7 have dysfunctional mitochondria, which has been linked to impaired CD8^{+} T-cell antitumor responses.

P2rx7$^{-/-}$ CD8^{+} T cells exhibit cell-intrinsic defects during the response to tumor.

Differences in initial tumor control by WT and *P2rx7*$^{-/-}$ CD8^{+} T cells could potentially affect the phenotype or function of these cells even at early time points, due to an altered TME. Hence, we next investigated whether differences seen for WT and *P2rx7*$^{-/-}$ CD8^{+} T cells would be recapitulated when both populations were present in the same TME. Equal numbers of WT and *P2rx7*$^{-/-}$ OT-I cells were co-transferred into mice with palpable B16.OVA tumors. This approach permitted evaluation of cell-intrinsic effects of P2RX7-deficiency, while the co-transferred WT cells are expected to limit tumor growth, allowing for evaluation at later time points after ACT. Seven and 18 days later, the ratio and phenotype of cells infiltrating the tumor, dLN and spleens of B16.OVA engrafted mice were analyzed. Between these time points, the tumor size increased considerably, as expected (Fig. 4a). At day 7, WT and *P2rx7*$^{-/-}$ OT-I cells were present at equal frequencies within the tumors and secondary lymphoid organs (SLO) (Fig 4b, Fig S4a). However, by day 18, we observed a preferential loss of P2rx7$^{-/-}$ OT-I cells within the tumor, dLN, and spleen (Fig 4b, Supplementary Fig S4a). Furthermore, although the frequency of cells expressing exhaustion markers was greater among the WT donor population at day 7, by d18 we observed increased expression of PD-1 and Lag3 by the *P2rx7*$^{-/-}$ OT-I population (Fig. 4c) and the *P2rx7*$^{-/-}$ populations showed impaired *ex vivo* production of IFNγ (Fig. 4d). The frequency of the TCF1^{+} 'stem-like' population within the tumor initially favored the *P2rx7*$^{-/-}$ population, but this advantage was lost by d18 (Supplementary Fig. S4b). At both time points, we observed significantly increased frequencies of Annexin V^{+} (LiveDead/PI^{-}) cells among the *P2rx7*$^{-/-}$ OT-I cells within the tumor (Fig 4e), suggesting these cells are preferentially undergoing apoptotic death, potentially contributing to the loss of *P2rx7*$^{-/-}$ cells by d18. *P2rx7*$^{-/-}$ OT-I in the tumor and dLN showed reduced proliferation (measured by Ki67 staining) at d7, and this defect was sustained in the dLN at d18 (Fig 4f). Finally, tumor-infiltrating *P2rx7*$^{-/-}$ displayed reduced expression of the "residency marker" CD103 within the tumor (Fig 4g), which may suggest impaired tumor residency. Taken together, these data suggest a progressive loss in function and maintenance among *P2rx7*$^{-/-}$ CD8^{+} T

cells as time and the tumor burden increase, resulting in increased cell death and reduced representation of *P2rx7*$^{-/-}$ CD8^{+} among tumor-infiltrating lymphocytes.

We also assessed the mitochondrial fitness of co-transferred WT and *P2rx7*$^{-/-}$ OT-I cells at both time points. At day 18, we observed a significant increase in frequency of *P2rx7*$^{-/-}$ OT-I cells with depolarized mitochondria within the tumor (Fig 5a). Additionally, consistent with our findings from the single-transfer model, we observed that WT OT-I cells within the tumor and dLN had higher mitochondrial mass and improved membrane potential and activity per mitochondrion at both time points (Fig. 5b–d), suggesting the impaired mitochondrial fitness observed for *P2rx7*$^{-/-}$ CD8^{+} T cells was cell-intrinsic. Additionally, *P2rx7*$^{-/-}$ CD8^{+} T cells within the tumor at d18 had significantly lower levels of mitochondrial ROS, consistent with mitochondrial function being reduced (Fig 5e). These results demonstrate that the *P2rx7*$^{-/-}$ CD8^{+} T-cell population is susceptible to varied mitochondrial defects even when the TME is normalized through the use of a co-transfer approach, indicating that this dysfunction is cell-intrinsic.

Metabolic differences between WT and *P2rx7*$^{-/-}$ CD8^{+} T cells arise during *in vitro* activation

It was unclear whether the mitochondrial defects observed in tumor-infiltrating *P2rx7*$^{-/-}$ CD8^{+} T cells were established during *in vitro* activation or were a result of cells encountering antigen in the hypoxic, nutrient-depleted TME. Furthermore, the impact of IL12 on the metabolic activity of cultured CD8^{+} T cells has not been clearly defined. We initially assessed oxidative phosphorylation and glycolysis in WT and *P2rx7*$^{-/-}$ P14 cells at 72h of stimulation, using extracellular flux ‘Seahorse’ assays. IL12 culture significantly increased the baseline and maximum OCR of WT P14 cells, but not *P2rx7*$^{-/-}$ P14 cells (Fig 6a–c), and it showed a trend toward increased SRC (Fig. 6d). Consistent with the metabolic defects in *P2rx7*$^{-/-}$ CD8^{+} T cells being primarily related to mitochondrial function, we observed no differences in glycolytic capacity of WT and *P2rx7*$^{-/-}$ CD8^{+} T cells, as measured by ECAR (Supplementary Fig. S5a–b).

We next determined how this related to mitochondrial homeostasis of *in vitro* cultured WT and *P2rx7*$^{-/-}$ P14 T cells. IL12 increased mitochondrial mass in both populations and the effect was significantly more potent for *P2rx7*$^{-/-}$ cells, yet mitochondrial membrane population was not elevated proportionally, such that IL12 exaggerated the differences in relative membrane potential (TMRE/MTG ratio) between WT and *P2rx7*$^{-/-}$ T cells (Fig 6e–g). These results illustrate the ability of IL12 to boost the levels of functional mitochondria in WT CD8^{+} T cells but not to the same extent in *P2rx7*$^{-/-}$ cells. These results mirror mitochondrial defects observed *in vivo* and suggest that *P2rx7*$^{-/-}$ P14 are disadvantaged metabolically prior to arrival in the TME, which may compromise the durability of the antitumor immune responses.

Augmentation of ACT by P2RX7 agonism

Our findings indicated that there may be an opportunity to boost ACT antitumor efficacy by stimulation of P2RX7 *in vitro* prior to cell transfer. We previously showed that stimulation of CD8^{+} T cells with the ATP analog BzATP, a P2RX7 agonist, leads to increased cell proliferation and Ca^{2+} influx, without compromising viability [8]. Here, we found that

BzATP treatment of $CD8^+$ T cells, in the absence of IL12, enhanced mitochondrial function, leading to increased OCR and SRC in WT but not *P2rx7*$^{-/-}$ $CD8^+$ T cells (Supplementary Fig. S6), but did not significantly change cell-surface expression of P2RX7 (Supplementary Fig. S2d). To test whether P2RX7 agonism could be used to enhance immunotherapy by $CD8^+$ T cells cultured in the absence of IL12, we activated P14 $CD8^+$ T cells *in vitro* for 72 hours with 3 doses of 100μM BzATP (added every 24 hours), or vehicle (H_2O) treatment, and then transferred these cells into mice bearing B16.gp33 tumors, without further BzATP treatment. We found that addition of BzATP during *in vitro* activation significantly improved survival and reduced tumor area in comparison to vehicle-treated P14 cells (Fig. 7a–c), albeit less effectively than IL12 cultured cells (Fig. 1). In parallel studies, we found that BzATP treatment had no effect on tumor control mediated by *P2rx7*$^{-/-}$ P14 cells, indicating the effect requires BzATP stimulation of P2RX7 (Supplementary Fig. S7a). To determine whether continued P2RX7 activity was needed to sustain antitumor activity, some animals were also treated with the P2RX7 antagonist A438074 (A438) *in vivo* every other day beginning at the time of T-cell transfer. As previously described in similar studies with P2RX7 antagonists [5, 6], A438 treatment had a modest beneficial effect on survival of mice that did not receive T cells. However, A438 treatment significantly compromised the ability of BzATP-treated donor WT P14 T cells to enhance survival (Supplementary Fig. S7b). Preliminary studies indicated that BzATP stimulation did not further enhance the efficacy of IL12 cultured WT P14 cells for tumor control (Supplementary Fig. S7c), which may indicate that these treatments operate in the same functional pathway.

To determine the effects of transient BzATP treatment on the phenotype and mitochondrial homeostasis of tumor-infiltrating lymphocytes, tumors from mice were harvested 7 days after T-cell transfer. We observed that BzATP treatment during *in vitro* activation led to reduced numbers of P14 cells per gram of tumor at the time of harvest (Supplementary Fig. S8a), but increased proliferation of those cells (Fig. 7d). It also reduced the frequency of P14 cells expressing the inhibitory receptors Tim3 (Fig. 7e), but not PD-1 (Supplementary Fig. S8b). Consistent with transient P2RX7 stimulation *in vitro* promoting mitochondrial function of tumor-infiltrating lymphocytes, BzATP-treated P14 cells in the tumor exhibited higher mitochondrial membrane potential and function per mitochondrion, despite no significant change in mitochondrial mass or change in frequency of $MTG^{hi}TMRE^{lo}$ cells (Fig. 7f–h, Supplementary Fig. S8c). However, BzATP-treated P14 cells in lymphoid tissues showed reduced mitochondrial mass and membrane potential (Fig. 7f–h), suggesting *in vitro* BzATP treatment may preferentially benefit mitochondrial function in tumor-infiltrating cells.

Together, these results demonstrate that P2RX7 stimulation is beneficial for $CD8^+$ T cell–mediated antitumor immunity and highlight the potential for P2RX7 stimulation of cultured $CD8^+$ T cells to promote tumor control.

Discussion

Previous studies have shown that mice that lack P2RX7 display accelerated tumor growth and have fewer tumor-infiltrating lymphocytes compared to WT mice [5, 6]. However, P2RX7 is expressed on many cell types, including various immune populations and many

tumors [7], making the cell-intrinsic role of P2RX7 difficult to discern from such studies. Indeed, expression of P2RX7 by tumor cells (including B16 melanoma) can contribute to their growth, as indicated by studies showing that P2RX7 pharmacological blockade limits tumor growth [5, 6]. The situation is further complicated by the capacity of high levels of eATP to transform P2RX7 signaling from a non-selective cation channel into generating a lethal macropore; the high eATP concentrations often found in the TME may therefore make P2RX7 expression a liability rather than a benefit for immune cells. Indeed, although we previously showed that P2RX7 expression is beneficial for the establishment and maintenance of $CD8^+$ memory T cells following responses to chronic and acute infections [8, 9], one study suggested that P2RX7 was detrimental for $CD8^+$ T cell–mediated tumor immunotherapy [10]. Nevertheless, it was not clear what role P2RX7 would play in adoptive immunotherapy by $CD8^+$ T cells that were optimally stimulated for efficient tumor control. In particular, our studies herein built on the observation that IL12 treatment of tumor-specific $CD8^+$ T cells during *in vitro* activation dramatically improves their persistence and ability to eradicate tumors [11]. Indeed, although our data indicate that P2RX7 expression offers no benefit for suboptimally-stimulated $CD8^+$ T cells, the enhanced tumor control induced by IL12 cultured $CD8^+$ T cells was severely blunted by P2RX7-deficiency. P2RX7 expression correlated with production of functional mitochondria in tumor infiltrating $CD8^+$ T cells, an effect that was also observed following *in vitro* activation prior to adoptive transfer.

As tumors expand, their increased metabolic demand creates an environment that is extremely hypoxic and depleted of nutrients. This poses an obstacle that infiltrating immune cells must adapt to in order to meet their own metabolic needs. Mitochondrial health and homeostasis is dependent on controlled biosynthesis and autophagic degradation of mitochondria [30]. These processes are often impaired in tumor-infiltrating $CD8^+$ T cells, resulting in poor mitochondrial quality and the accumulation of damaged mitochondria compared to splenic $CD8^+$ T cells [17, 31]. Consistent with those studies, we found that mitochondria in tumor-infiltrating $CD8^+$ T cells had a lower mitochondrial membrane potential and an increased frequency of depolarized mitochondria. These characteristics were significantly worsened in *P2rx7*$^{-/-}$ $CD8^+$ T cells within the tumor. P2RX7-deficient $CD8^+$ T cells also showed mitochondrial impairments and reduced baseline and maximum levels of OXPHOS after *in vitro* activation. The glycolytic capacity of *in vitro* activated *P2rx7*$^{-/-}$ $CD8^+$ T cells was not impaired compared to WT $CD8^+$ T cells. T cells shift their metabolism to predominately utilize aerobic glycolysis upon activation [32]. P2RX7-deficient $CD8^+$ T cells may be able to compensate for mitochondrial defects initially by relying on glycolysis, but likely lack the plasticity necessary to adapt to changes in nutrient and oxygen availability in the TME.

Metabolic alternations in tumor-infiltrating $CD8^+$ T cells are early events that ultimately lead to T-cell exhaustion [31, 33, 34]. Furthermore, manipulation of $CD8^+$ T cells to optimize mitochondrial function and structure correlates with reduced expression of inhibitory receptors [35–37] and can even restore functionality of exhausted T cells [18, 38]. Consistent with this, we found that intratumoral *P2rx7*$^{-/-}$ $CD8^+$ T cells exhibited increased expression of some exhaustion markers and reduced production of IFNγ as the antitumor response progressed. These changes occurred alongside continued mitochondrial

dysfunction and correlate with selective loss of *P2rx7*$^{-/-}$ CD8^{+} T cells within the tumor and dLN. These data reinforce the strong link between mitochondrial fitness and T-cell function and survival. Our data also indicate that mitochondrial function may in some cases be an early indicator of an effective T-cell antitumor response before the onset of exhaustion.

Although our data suggest that the role of P2RX7 in promoting CD8^{+} T-cell responses and metabolic fitness is similar in the context of acute/chronic infections and tumors [8, 9], the numeric defect among tumor-infiltrating *P2rx7*$^{-/-}$ CD8^{+} T cells was more subtle than our observations in infection models [8, 9]. This may relate to the early time points of analysis required for studies involving the rapidly growing B16 model, but it is also possible that this finding relates to the dual functions of P2RX7: While P2RX7-deficiency may compromize mitochondrial maintenance, overstimulation of P2RX7, due to high expression levels or elevated concentrations of eATP in the TME may induce P2RX7 to form a macropore resulting in death of WT T cells [1, 39, 40]. In normal tissues, eATP concentrations are in the nM range, but in the TME, eATP concentrations can reach hundeds of μM [3]. P2RX7 macropore formation can also be induced by NAD-mediated ribosylation of P2RX7 by the ectoenzzyme ARTC2.2 [2]. For this reason, we used nanobody-mediated ARTC2.2 antagonism at the time of harvest, which we have shown improves recovery of P2RX7-expressing CD8^{+} T cells during tissue processing where NAD might be released from necrotic cells [41]. However, this does not protect P2RX7-expressing T cells from high concentrations of eATP within the tumor *in vivo*. For these reasons, it is likely that the TME may be especially hostile to P2RX7-expressing WT CD8^{+} T cells, yet our data indicate that this is outweighed by their improved ability to control tumor growth. Still, given the complicated nature of P2RX7 signaling, particularly in high eATP/NAD environments where the receptor could be a liability, it is not suprising that there is some discrepancy on the cell-intrinsic role of P2RX7 in the context of CD8^{+} ACT. Furthemore, P2RX7 may have a distinct role on CD4^{+} T cells, where its expression may promote survival of regulatory T cells [1]. Indeed, Romagnani et al. observed that P2RX7-deficiency was advantageous for CD4^{+} T-cell survival and tumor control [10]. Nevertheless, our findings suggest a need for careful evaluation of how tumor-specific T cells are activated in order to address whether P2RX7 plays a beneficial versus a detrimental role.

In summary, we report that P2RX7-deficient CD8^{+} T cells exhibit increased mitochondrial dysfunction, reduced proliferation, increased levels of apoptosis, and elevated expression of exhaustion markers as tumor burden increases, leading to loss of *P2rx7*$^{-/-}$ CD8^{+} donor cells within the tumor and in secondary lymphoid organs. We conclude that these combined defects account for impaired tumor control when *P2rx7*$^{-/-}$ CD8^{+} T cells are used for ACT. Strategies to boost mitochondrial health CD8^{+} tumor-infiltrating lymphocytes have shown to improve T-cell survival and function under metabolic stressors imposed by the TME [36, 42]. Consistent with those studies, we report that transient P2RX7 agonism (with BzATP) increased mitochondrial mass and function in tumor-infiltrating WT CD8^{+} T cells resulting in enhanced tumor control.These data demonstrate that stimulation of the P2RX7 signaling pathway is a promising therapeutic option that could easily be optimized and incorporated into existing ACT protocols. Futhermore, the requirement for P2RX7 to generate an effective antitumor response has clinical relevance as P2RX7 loss-of-function variants are relatively common in the human population [43] and patients with those

mutations may require ACT protocols that boost the mitochondrial health of transferred T cells.

Supplementary Material

Refer to Web version on PubMed Central for supplementary material.

Acknowledgements

We thank Ananda Goldrath (UCSD) and Matthew Mescher (UMN) for providing us with the B16.gp33 and B16.OVA cell lines, respectively and thank Peter Hinderlie and Jeffrey Miller (UMN) for their assistance with the Incucyte assays. We appreciate all members of the Jamequist lab for input on these studies and critical comments on the manuscript. This work was supported by the NIH (R01 AI145147 to S.C.J.; R00 AI139381 to H.BdS.; F30 CA250231 to K.M.W.) and H.BdS. was supported by a Paul C. Shiverick/CRI Irvington fellowship.

Funding:

This work was supported by the NIH (R01 AI145147 to S.C.J.; R00 AI139381 to H.BdS.; F30 CA250231 to K.M.W.) and H.BdS. was supported by a Paul C. Shiverick/CRI Irvington fellowship.

References

1. Di Virgilio F, et al. , The P2X7 Receptor in Infection and Inflammation. Immunity, 2017. 47(1): p. 15–31. [PubMed: 28723547]
2. Rissiek B, et al. , P2X7 on Mouse T Cells: One Channel, Many Functions. Front Immunol, 2015. 6: p. 204. [PubMed: 26042119]
3. Pellegatti P, et al. , Increased level of extracellular ATP at tumor sites: in vivo imaging with plasma membrane luciferase. PLoS One, 2008. 3(7): p. e2599. [PubMed: 18612415]
4. Ghiringhelli F, et al. , Activation of the NLRP3 inflammasome in dendritic cells induces IL-1beta-dependent adaptive immunity against tumors. Nat Med, 2009. 15(10): p. 1170–8. [PubMed: 19767732]
5. Adinolfi E, et al. , Accelerated tumor progression in mice lacking the ATP receptor P2X7. Cancer Res, 2015. 75(4): p. 635–44. [PubMed: 25542861]
6. De Marchi E, et al. , The P2X7 receptor modulates immune cells infiltration, ectonucleotidases expression and extracellular ATP levels in the tumor microenvironment. Oncogene, 2019.
7. Di Virgilio F, et al. , Extracellular ATP and P2 purinergic signalling in the tumour microenvironment. Nat Rev Cancer, 2018.
8. Borges da Silva H, et al. , The purinergic receptor P2RX7 directs metabolic fitness of long-lived memory CD8. Nature, 2018. 559(7713): p. 264–268. [PubMed: 29973721]
9. Borges da Silva H, et al. , Sensing of ATP via the Purinergic Receptor P2RX7 Promotes CD8. Immunity, 2020. 53(1): p. 158–171.e6. [PubMed: 32640257]
10. Romagnani A, et al. , P2X7 Receptor Activity Limits Accumulation of T Cells within Tumors. Cancer Res, 2020. 80(18): p. 3906–3919. [PubMed: 32699136]
11. Gerner MY, et al. , Cutting edge: IL-12 and type I IFN differentially program CD8 T cells for programmed death 1 re-expression levels and tumor control. J Immunol, 2013. 191(3): p. 1011–5. [PubMed: 23804712]
12. Tucker CG, et al. , Adoptive T Cell Therapy with IL-12-Preconditioned Low-Avidity T Cells Prevents Exhaustion and Results in Enhanced T Cell Activation, Enhanced Tumor Clearance, and Decreased Risk for Autoimmunity. J Immunol, 2020. 205(5): p. 1449–1460. [PubMed: 32737148]
13. Rosenberg SA and Restifo NP, Adoptive cell transfer as personalized immunotherapy for human cancer. Science, 2015. 348(6230): p. 62–8. [PubMed: 25838374]
14. June CH, et al. , CAR T cell immunotherapy for human cancer. Science, 2018. 359(6382): p. 1361–1365. [PubMed: 29567707]

15. Topalian SL, Drake CG, and Pardoll DM, Immune checkpoint blockade: a common denominator approach to cancer therapy. Cancer Cell, 2015. 27(4): p. 450–61. [PubMed: 25858804]
16. Buck MD, et al. , Mitochondrial Dynamics Controls T Cell Fate through Metabolic Programming. Cell, 2016. 166(1): p. 63–76. [PubMed: 27293185]
17. Scharping NE, et al. , The Tumor Microenvironment Represses T Cell Mitochondrial Biogenesis to Drive Intratumoral T Cell Metabolic Insufficiency and Dysfunction. Immunity, 2016. 45(3): p. 701–703. [PubMed: 27653602]
18. Scharping NE, et al. , Mitochondrial stress induced by continuous stimulation under hypoxia rapidly drives T cell exhaustion. Nat Immunol, 2021. 22(2): p. 205–215. [PubMed: 33398183]
19. Yu YR, et al. , Disturbed mitochondrial dynamics in $CD8^+$ TILs reinforce T cell exhaustion. Nat Immunol, 2020. 21(12): p. 1540–1551. [PubMed: 33020660]
20. Kishton RJ, Sukumar M, and Restifo NP, Metabolic Regulation of T Cell Longevity and Function in Tumor Immunotherapy. Cell Metab, 2017. 26(1): p. 94–109. [PubMed: 28683298]
21. Martínez-García JJ, et al. , P2X7 receptor induces mitochondrial failure in monocytes and compromises NLRP3 inflammasome activation during sepsis. Nat Commun, 2019. 10(1): p. 2711. [PubMed: 31221993]
22. van der Windt GJ, et al. , Mitochondrial respiratory capacity is a critical regulator of CD8+ T cell memory development. Immunity, 2012. 36(1): p. 68–78. [PubMed: 22206904]
23. Lee JY, et al. , The transcription factor KLF2 restrains $CD4^+$ T follicular helper cell differentiation. Immunity, 2015. 42(2): p. 252–264. [PubMed: 25692701]
24. Schmidt R, et al. , CRISPR activation and interference screens decode stimulation responses in primary human T cells. Science, 2022. 375(6580): p. eabj4008. [PubMed: 35113687]
25. Stark R, et al. , TRM maintenance is regulated by tissue damage via P2RX7. Sci Immunol, 2018. 3(30).
26. Schenkel JM, et al. , Conventional type I dendritic cells maintain a reservoir of proliferative tumor-antigen specific TCF-1. Immunity, 2021. 54(10): p. 2338–2353.e6. [PubMed: 34534439]
27. Molodtsov AK, et al. , Resident memory $CD8^+$ T cells in regional lymph nodes mediate immunity to metastatic melanoma. Immunity, 2021. 54(9): p. 2117–2132.e7. [PubMed: 34525340]
28. Connolly KA, et al. , A reservoir of stem-like CD8+ T cells in the tumor-draining lymph node preserves the ongoing antitumor immune response. Sci Immunol, 2021. 6(64): p. eabg7836. [PubMed: 34597124]
29. Rivadeneira DB and Delgoffe GM, Antitumor T-cell Reconditioning: Improving Metabolic Fitness for Optimal Cancer Immunotherapy. Clin Cancer Res, 2018. 24(11): p. 2473–2481. [PubMed: 29386217]
30. Beckermann KE, Dudzinski SO, and Rathmell JC, Dysfunctional T cell metabolism in the tumor microenvironment. Cytokine Growth Factor Rev, 2017. 35: p. 7–14. [PubMed: 28456467]
31. Yu YR, et al. , Disturbed mitochondrial dynamics in CD8. Nat Immunol, 2020. 21(12): p. 1540–1551. [PubMed: 33020660]
32. Pearce EL, et al. , Fueling immunity: insights into metabolism and lymphocyte function. Science, 2013. 342(6155): p. 1242454. [PubMed: 24115444]
33. Bengsch B, et al. , Bioenergetic Insufficiencies Due to Metabolic Alterations Regulated by the Inhibitory Receptor PD-1 Are an Early Driver of CD8(+) T Cell Exhaustion. Immunity, 2016. 45(2): p. 358–73. [PubMed: 27496729]
34. Gu M, et al. , NF-κB-inducing kinase maintains T cell metabolic fitness in antitumor immunity. Nat Immunol, 2021. 22(2): p. 193–204. [PubMed: 33398181]
35. Kawalekar OU, et al. , Distinct Signaling of Coreceptors Regulates Specific Metabolism Pathways and Impacts Memory Development in CAR T Cells. Immunity, 2016. 44(3): p. 712.
36. Menk AV, et al. , 4-1BB costimulation induces T cell mitochondrial function and biogenesis enabling cancer immunotherapeutic responses. J Exp Med, 2018. 215(4): p. 1091–1100. [PubMed: 29511066]
37. Long AH, et al. , 4-1BB costimulation ameliorates T cell exhaustion induced by tonic signaling of chimeric antigen receptors. Nat Med, 2015. 21(6): p. 581–90. [PubMed: 25939063]

38. Chamoto K, et al. , Mitochondrial activation chemicals synergize with surface receptor PD-1 blockade for T cell-dependent antitumor activity. Proc Natl Acad Sci U S A, 2017. 114(5): p. E761–E770. [PubMed: 28096382]

39. Proietti M, et al. , ATP-gated ionotropic P2X7 receptor controls follicular T helper cell numbers in Peyer's patches to promote host-microbiota mutualism. Immunity, 2014. 41(5): p. 789–801. [PubMed: 25464855]

40. Aswad F, Kawamura H, and Dennert G, High sensitivity of CD4+CD25+ regulatory T cells to extracellular metabolites nicotinamide adenine dinucleotide and ATP: a role for P2X7 receptors. J Immunol, 2005. 175(5): p. 3075–83. [PubMed: 16116196]

41. Borges da Silva H, et al. , ARTC2.2/P2RX7 Signaling during Cell Isolation Distorts Function and Quantification of Tissue-Resident CD8. J Immunol, 2019. 202(7): p. 2153–2163. [PubMed: 30777922]

42. Teijeira A, et al. , Mitochondrial Morphological and Functional Reprogramming Following CD137 (4-1BB) Costimulation. Cancer Immunol Res, 2018. 6(7): p. 798–811. [PubMed: 29678874]

43. Fuller SJ, et al. , Genetics of the P2X7 receptor and human disease. Purinergic Signal, 2009. 5(2): p. 257–62. [PubMed: 19319666]

Synopsis:

The role of the purinergic receptor P2RX7 in $CD8^+$ T cell–mediated antitumor immunity has been equivocal. The authors show it supports mitochondrial function and survival of $CD8^+$ T cells during adoptive cell immunotherapy in a melanoma model.

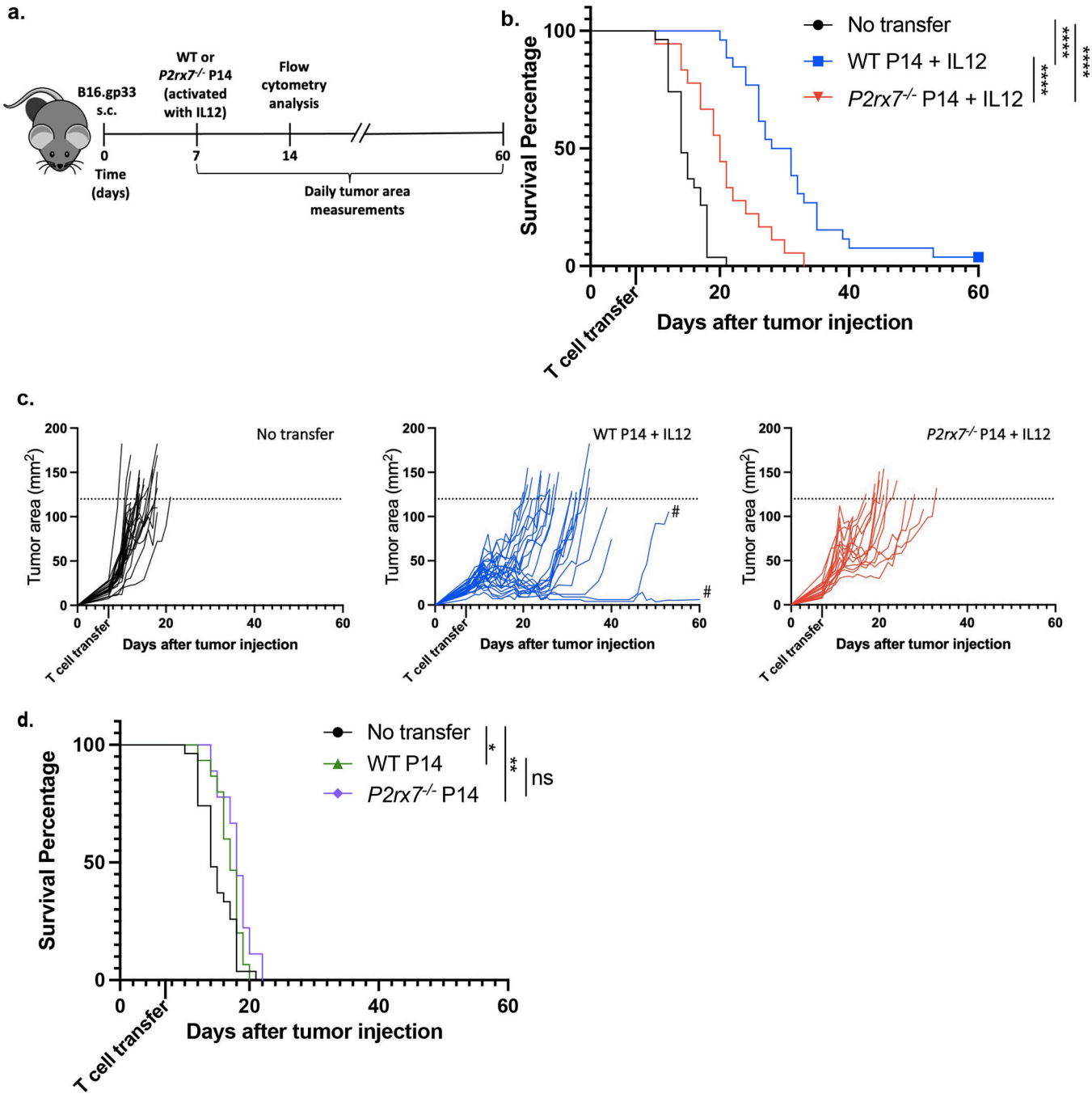

Fig. 1: P2RX7 is required for IL12-primed CD8$^+$ T cells to effectively control tumors.

a) C57BL/6 or B6.SJL mice were injected with 3×10^5 B16.gp33 melanoma cells subcutaneously. and once tumors became palpable (~7 days post-injection) 5×10^5 WT or *P2rx7*$^{-/-}$ P14 cells were transferred i.v. after 72 hours activation with anti-CD3/-CD28 and 2.5 IU/mL IL2, with (**b**-**c**) or without (**d**) 5 ng/mL IL12. **b)** Survival curve and **c)** tumor growth curves for individual tumor-bearing mice that received no cell transfer (n=27), WT P14 cells (n=23), or *P2rx7*$^{-/-}$ P14 cells (n=18) activated with IL12 priming. **d)** Survival curve for tumor-bearing mice that received WT (n=15) or *P2rx7*$^{-/-}$ (n=9) P14 cells activated

without IL12. Endpoint criteria for survival experiments were tumor ulceration or an area of 120mm^2 (indicated by dashed line). Data are from 2–3 independent experiments. Bars show mean ± SEM. *, $P \leq 0.05$; **, $P \leq 0.01$; ***, $P \leq 0.001$; ****, $P \leq 0.0001$. Statistical significance for **b, d** determined by a log-rank Mantel-Cox test.

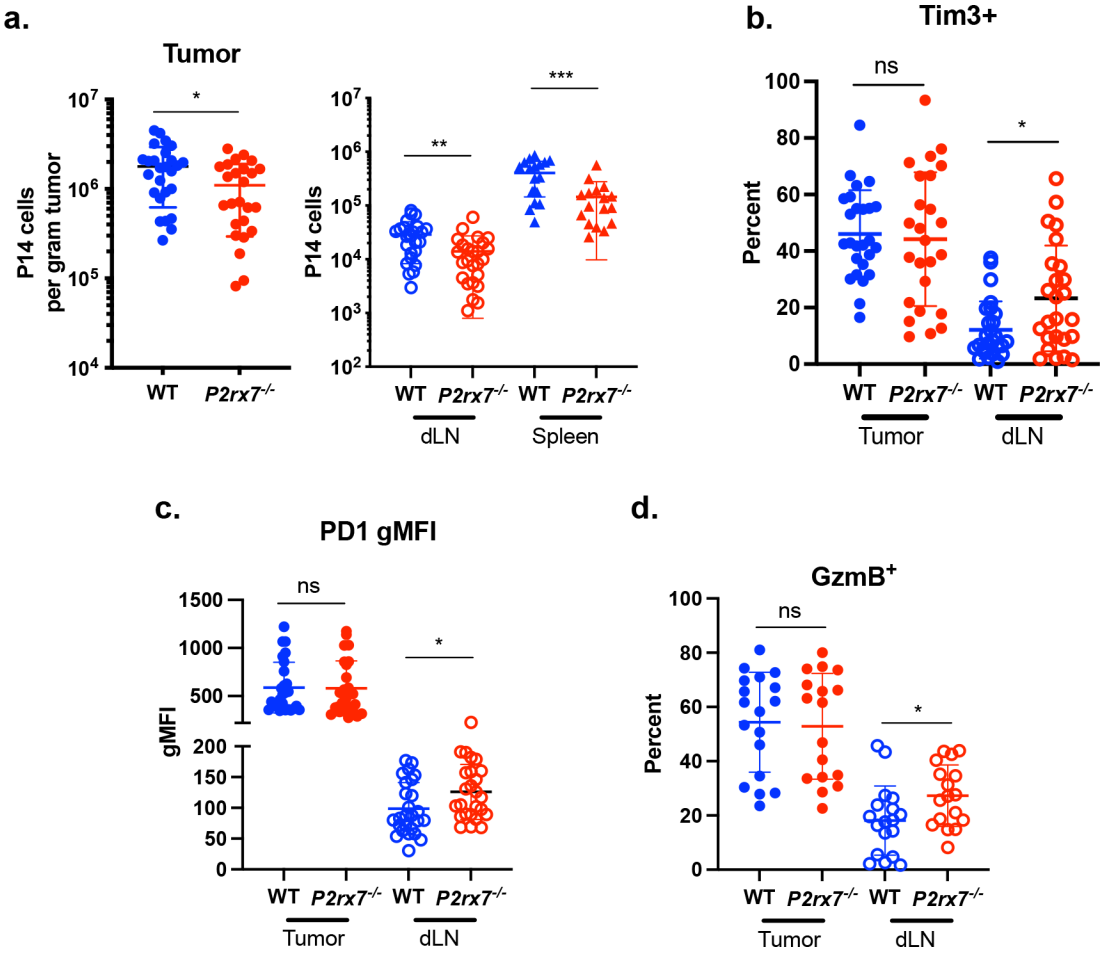

Fig. 2: Tumor-specific *P2rx7*$^{-/-}$ CD8^{+} T cells within dLN have increased expression of exhaustion markers.

WT or *P2rx7*$^{-/-}$ P14 cells (activated in the presence of IL12) were transferred into C57BL/6 or B6.SJL with palpable B16.gp33 tumors. Tumors, tumor dLNs, and spleens were harvested from recipient mice 7 days after T-cell transfer. **a)** Number of live P14 cells per gram tumor and within dLN and spleen. **b)** Percentage of Tim3^{+} P14 cells within tumor (left) and dLN (right). **c)** PD1 gMFI of P14 cells within tumor (left) and dLN (right). **d)** Percentage of GzmB^{+} P14 cells post-*ex vivo* restimulation with PMA/Ionomycin. Data are from 3–4 independent experiments with 25 mice per group. Graphical data shown as means with error bars indicating SEM. *, $P \leq 0.05$; **, $P \leq 0.01$; ***, $P \leq 0.001$. Statistical significance determined by a two-tailed, unpaired t-test.

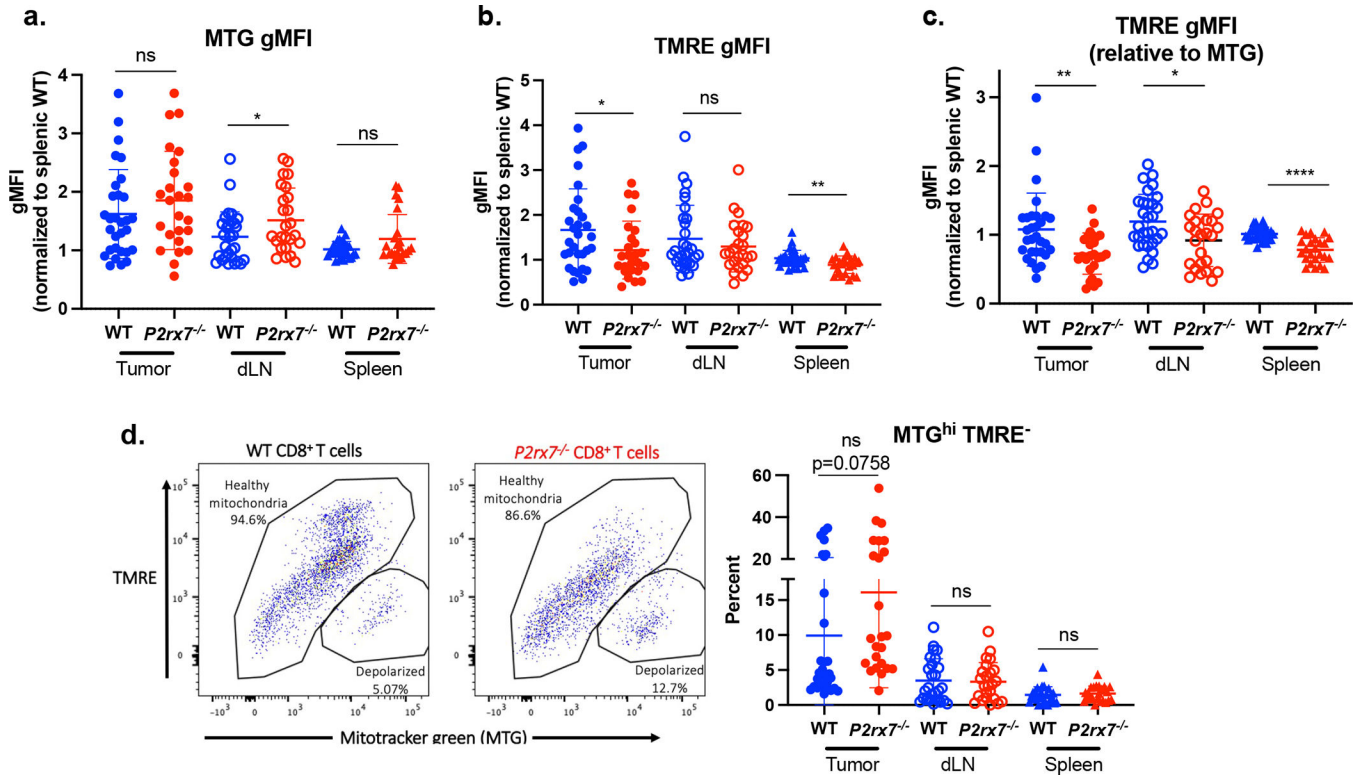

Fig. 3: *P2rx7*$^{-/-}$ CD8^{+} T cells show signs of mitochondrial dysfunction.

Activated WT or *P2rx7*$^{-/-}$ P14 cells were cultured with IL12 then transferred into C57BL/6 or B6.SJL bearing palpable B16.gp33 tumors. Tumors, tumor dLNs and spleens were harvested from recipient mice 7 days after T-cell transfer. Mitochondrial mass and membrane potential were measured in WT and *P2rx7*$^{-/-}$ P14 cells within tumors of B16.gp33-engrafted mice by MTG and TMRE gMFI, respectively. Fold changes of **a)** MTG gMFI, **b)** TMRE gMFI, **c)** relative TMRE gMFI (normalized to MTG gMFI). **(a-c)** For each independent experiment, fold change in gMFI for the indicated molecular probe was calculated relative to average gMFI of donor WT P14 cells within the spleen. **d)** Frequency of P14 cells with depolarized (MTG^{hi}TMRE^{lo}) mitochondria. Data are from 3 independent experiments with 25 mice per group. Graphical data shown as means with error bars indicating SEM. *, $P \leq 0.05$; **, $P \leq 0.01$; ***, $P \leq 0.001$; ****, $P \leq 0.0001$. Statistical significance determined by a two-tailed, unpaired t-test.

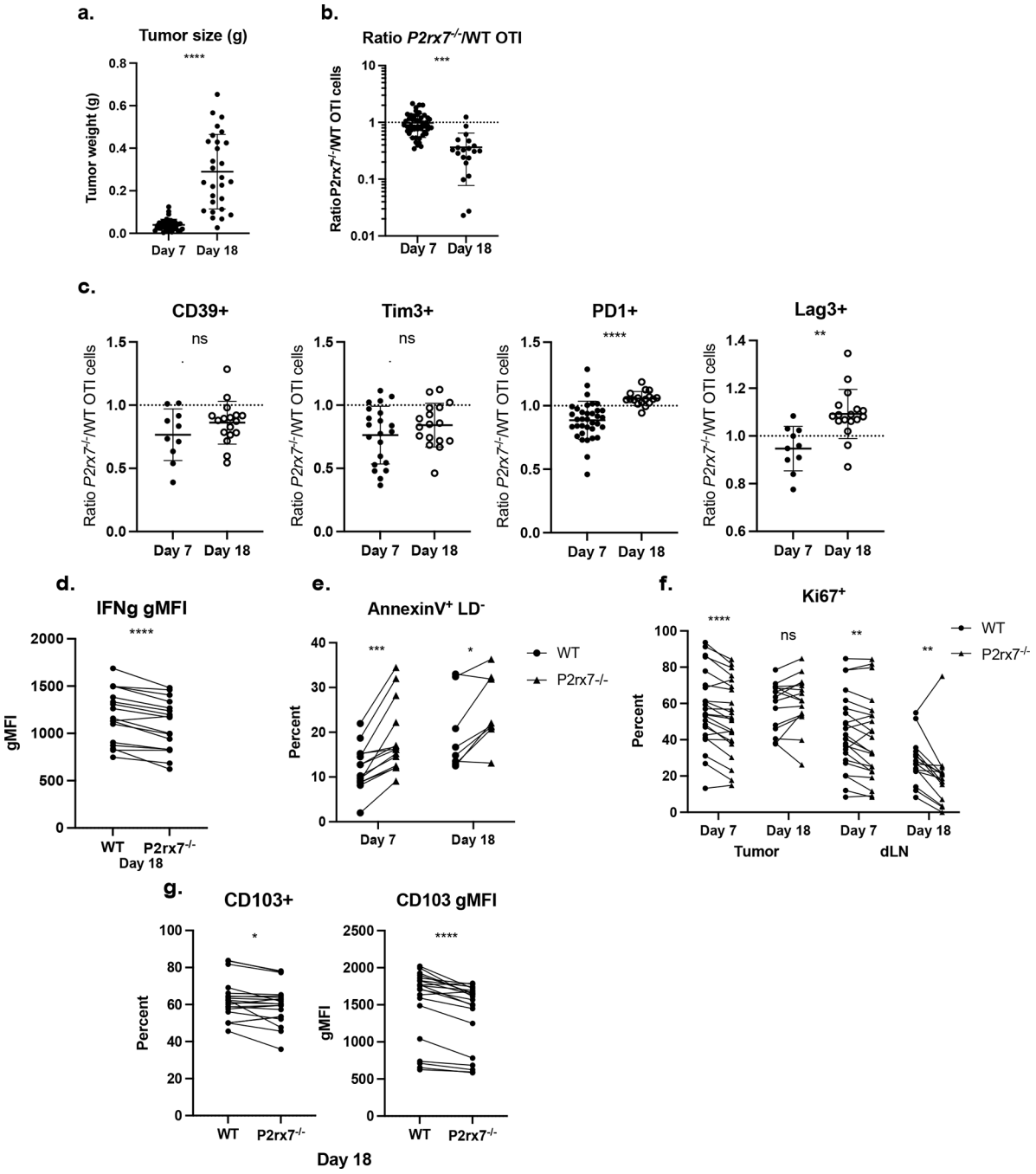

Fig. 4: Cell-intrisic defects in *P2rx7*$^{-/-}$ CD8^{+} T cells responding to tumor growth.

Equal numbers of activated WT and *P2rx7*$^{-/-}$ OT-I cells (activated with IL12) were co-transferred into C57BL/6 or B6.SJL with palpable B16.OVA tumors. Tumors, tumor dLNs, and spleens were harvested from recipient mice 7 and 18 days after T-cell transfer. **a)** Weight of tumors from B16.OVA engrafted mice at indicated time of harvest. **b)** Ratio *P2rx7*$^{-/-}$/WT OT-I donor cells within tumor at days 7 and 18 after T-cell transfer. **c)** Frequency of donor WT or *P2rx7*$^{-/-}$ OT-I cells that express (from left) CD39, Tim3, PD1, and Lag3 at each time point was determined and ratio *P2rx7*$^{-/-}$/WT OT-I cells within each population

was calculated to indicate change in expression of each marker at day 7 versus day 18. **d)** *Ex vivo* expression of IFNγ in WT versus *P2rx7*$^{-/-}$ OT-I cells from tumors of mice harvested at day 18. **e)** Frequency of apoptotic donor OT-I cells based on Annexin V^{+} and propidium iodide^{-} (PI) and LiveDead^{-} (LD). **f)** Frequency of proliferating (Ki67^{+}) donor cells within tumor and tumor dLN. **g)** Frequency of OT-I donor cells within the tumors of mice harvested at day 18 that express CD103 (left) and expression levels (right). Fold changes were calculated by normalizing the average gMFI of the indicated molecular probe in splenic T cells. Data are from 2–4 independent experiments with 10–48 mice per group. *, $P \leq 0.05$; **, $P \leq 0.01$; ***, $P \leq 0.001$; ****, $P \leq 0.0001$. Statistical significance determined by a two-tailed, paired t-test.

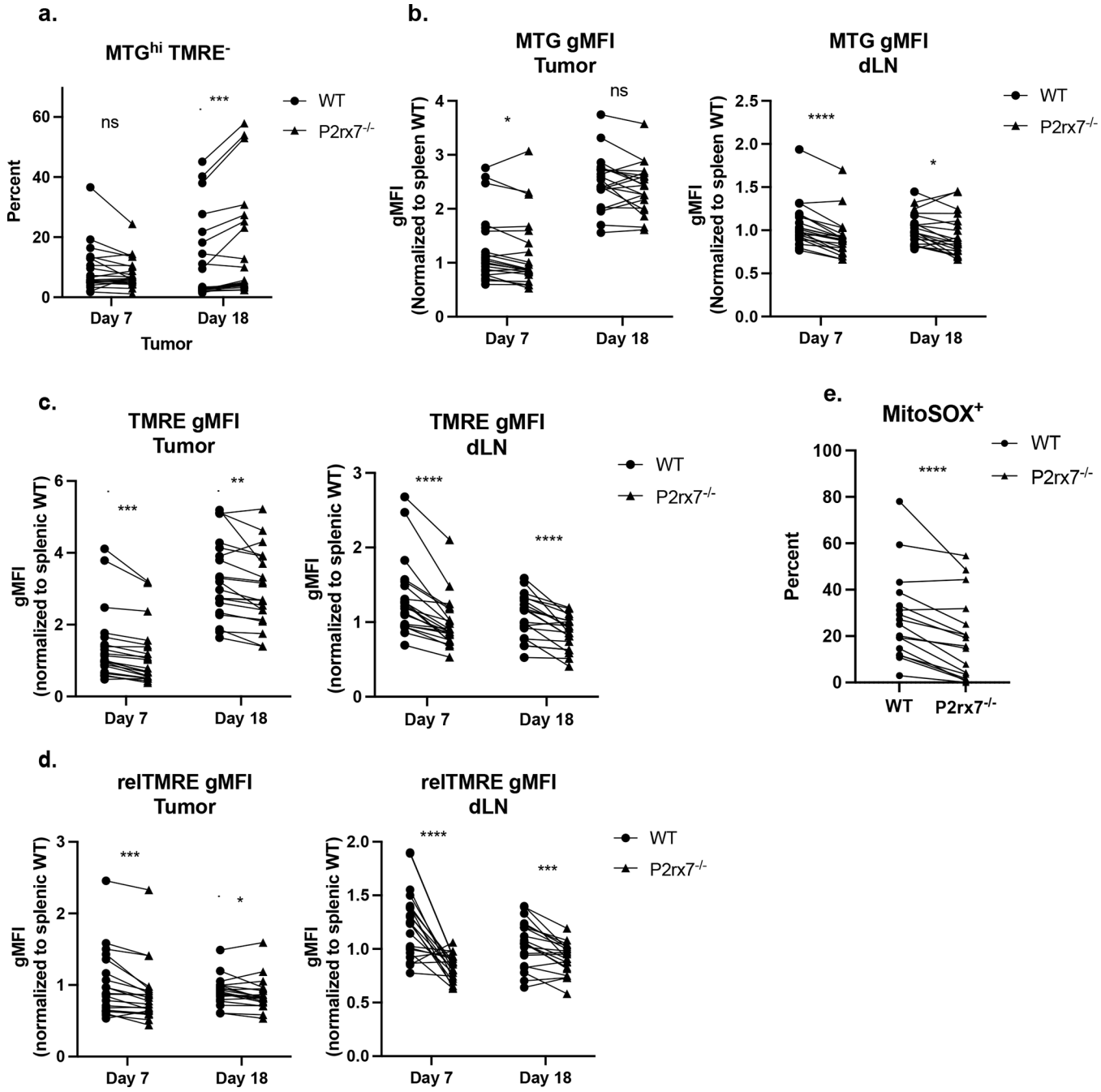

Fig. 5: Impaired mitochondrial fitness of *P2rx7*$^{-/-}$ CD8^{+} T cells is cell-intrinsic.

Equal numbers of WT and *P2rx7*$^{-/-}$ OT-I CD8^{+} T cells were activated in the presence of IL12 and equal numbers of cells were co-transferred into mice with palpable B16.OVA tumors. Tumors, tumor dLNs, and spleens were harvested from recipient mice 7 and 18 days after T-cell transfer. **a)** Frequency of OT-I donor cells with depolarized (MTG^{hi}TMRE^{lo}) mitochondria within the tumors of mice harvested at days 7 or 18. Fold changes of **b)** MTG gMFI, **c)** TMRE gMFI, **d)** relative TMRE gMFI (normalized to MTG gMFI) in OT-I donor cells from tumors and dLN at indicated time points.**(b-d)** For each independent experiment,

fold change in gMFI of indicated molecular probe was calculated relative to average gMFI of donor WT P14 cells within the spleen. **e)** Frequency of OT-I donor cells producing mitochodrial ROS, as indicated by MitoSOX^{+}, within tumors harvested at day 18. Data are from 3–4 independent experiments with 17–21 mice per group. *, $P \leq 0.05$; **, $P \leq 0.01$; ***, $P \leq 0.001$; ****, $P \leq 0.0001$. Statistical significance determined by a two-tailed, paired t-test.

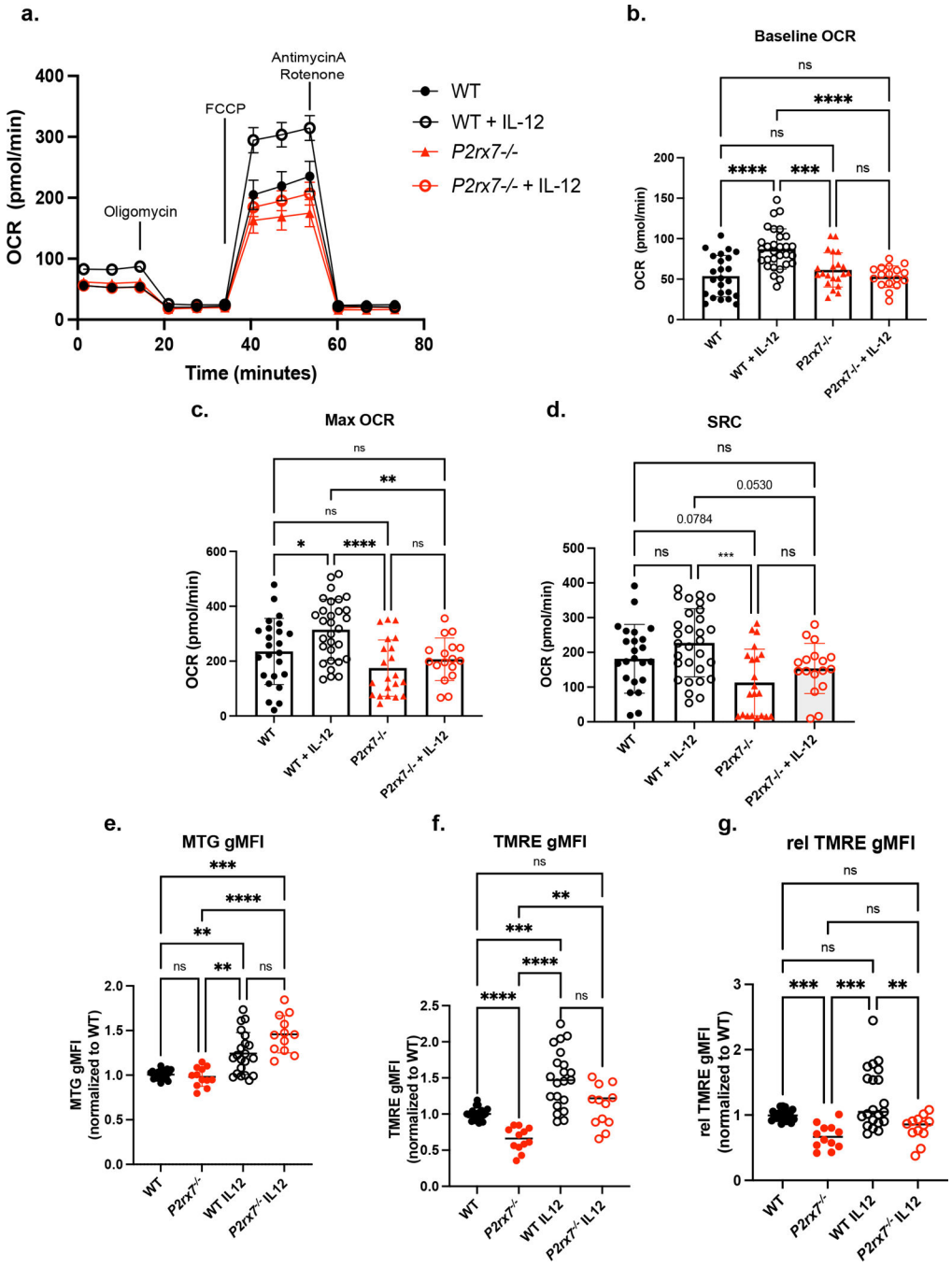

Fig. 6: Metabolic defects in *P2rx7*$^{-/-}$ CD8^{+} T cells arise during *in vitro* activation.

WT and *P2rx7*$^{-/-}$ P14 cells were activated for 72 hours *in vitro* with anti-CD3, anti-CD28, IL2, and +/− IL12. **(a-d)** Oxygen consumption rate (OCR) of indicated groups after 72 hour activation was evaluated using Seahorse Extracellular Flux assay. **a)** OCRs were determined for the indicated groups after sequential addition of the listed inhibitors. **b)** Baseline OCR of indicated groups (determined prior to Oligomycin addition). **c)** Maximum OCR of indicated groups (determined after FCCP addition). **d)** Spare respiratory capacity (SRC) of indicated groups (calculated based on difference between Max OCR and baseline

OCR). **(e-g)** Mitochondrial mass and membrane potential was measured in WT and *P2rx7*$^{-/-}$ P14 cells after *in vitro* activation by evaluating levels of MTG or TMRE, respectively. Fold changes of **e)** MTG gMFI, **f)** TMRE gMFI, and **g)** relative TMRE gMFI (normalized to MTG gMFI). **(e-g)** For each independent experiment, fold change in gMFI of indicated molecular probe was calculated relative to average gMFI of WT (untreated) P14 cells. Data are from 3–5 independent experiments. Graphical data shown as means with error bars indicating SEM. *, $P \leq 0.05$; **, $P \leq 0.01$; ***, $P \leq 0.001$; ****, $P \leq 0.0001$. Statistical significance determined by One-way ANOVA.

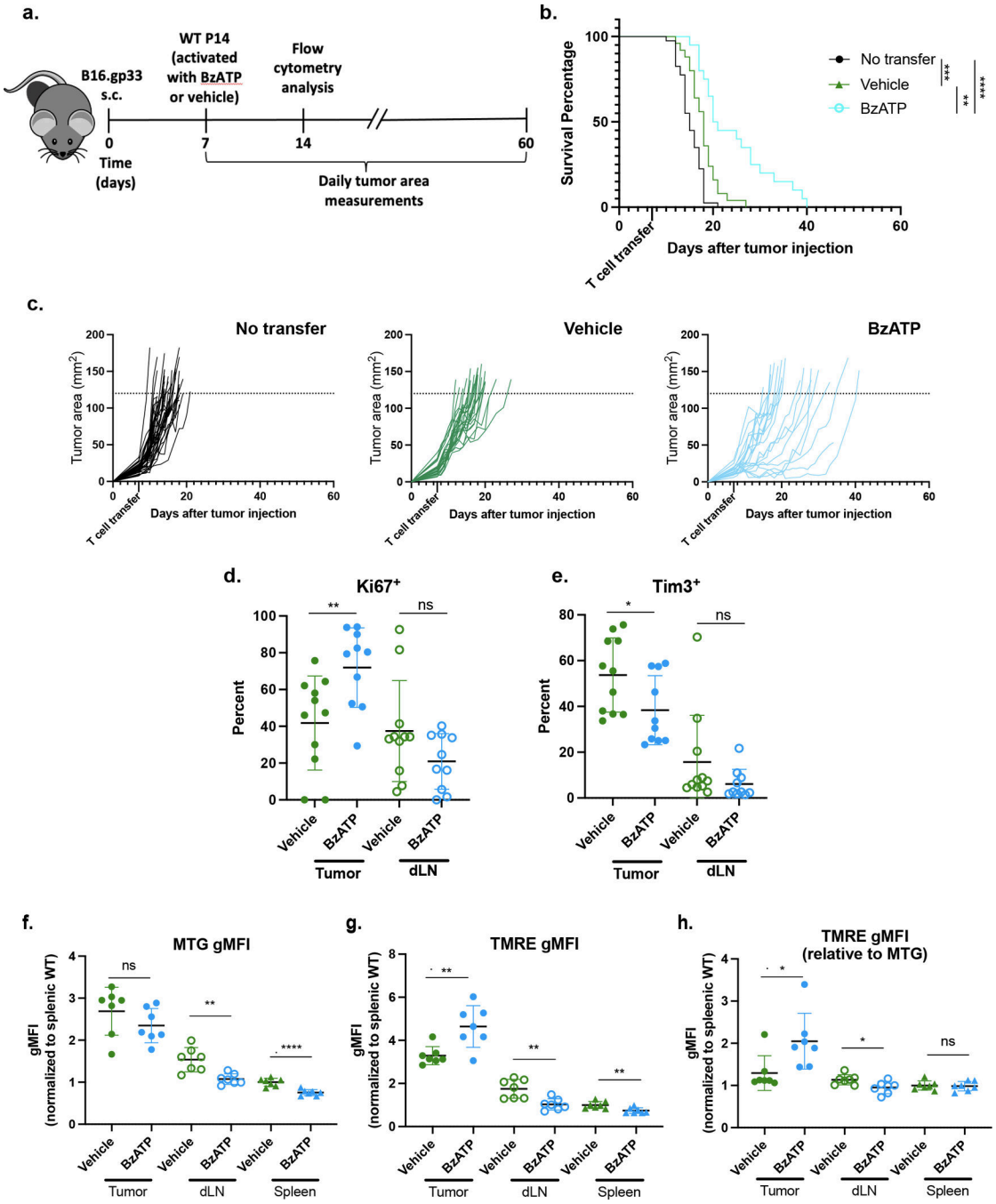

Fig. 7: P2RX7 agonism during *in vitro* activation improves survival and tumor control of WT CD8$^+$ T cells.

a) C57BL/6 or B6.SJL were injected with 3×10^5 B16.gp33 melanoma subcutaneously and once tumors became palpable (~7 days post-injection) 5×10^5 P14 cells were transferred i.v. after 72 hours activation with anti-CD3/-CD28, 2.5 IU/mL IL2, and +/− 100uM of BzATP (or vehicle dH_2O treatment) every 24 hours of activation. **b)** Survival curves and **c)** tumor growth curves for tumor-bearing mice that received vehicle-treated WT P14 cells (n=25), BzATP-treated WT P14 (n=20), or no T-cell transfer (n=40). **(d-h)** Tumors, tumor dLN and

spleens from mice with B16.gp33 tumors that received either vehicle- or BzATP-treated WT P14 donor cells were harvested at day 7 after T-cell transfer to determine: **d)** frequency of $Ki67^+$ P14 cells; **e)** frequency of $Tim3^+$ P14 cells; **f)** mitochondrial mass (MTG staining gMFI); **g)** mitochondrial membrane potential (TMRE gMFI), and **h)** relative TMRE gMFI. In **f-h**), values were normalized to vehicle-treated WT P14 cells in the spleen. **(f-h)** For each independent experiment, fold change in gMFI of indicated molecular probe was calculated relative to average gMFI of vehicle-treated WT P14 cells within the spleen. **(b-c)** Endpoint criteria for survival experiments were tumor ulceration or an area of $120mm^2$ (indicated by dashed line). Data are from 3 independent experiments. Graphical data shown as means with error bars indicating SEM. *, $P \leq 0.05$; **, $P \leq 0.01$; ***, $P \leq 0.001$; ****, $P \leq 0.0001$. Statistical significance for **b** determined by a log-rank Mantel–Cox test. Statistical significance for **d-h** evaluated by a two-tailed, unpaired t-test.

KEY RESOURCES TABLE

REAGENT or RESOURCE	SOURCE	IDENTIFIER
Antibodies/Flow Cytometry Dyes		
Anti-mouse CD8a BUV395 (53-6.7)	BD Biosciences	Cat# 563786, RRID: AB_2732919
Anti-mouse CD8a BUV496 (53-6.7)	BD Biosciences	Cat# 750024,, RRID: AB_2874242
Anti-Mouse CD45.1 violetFluor 450 (A20)	Tonbo Biosciences	Cat# 75-0453, RRID:AB_2621949
Anti-Mouse CD45.1 BUV395 (A20)	BD Biosciences	Cat# 565212, RRID:AB_2722493
Anti-Mouse CD45.2 violetFluor 450 (104)	Tonbo Biosciences	Cat# 75-0454, RRID:AB_2621950
Anti-Mouse CD45.2 BUV737 (104)	BD Biosciences	Cat# 564880, RRID:AB_2738998
Anti-Mouse CD45.2 FITC (104)	Tonbo Biosciences	Cat# 35-0454, RRID:AB_2621692
Anti-mouse CD44 BV786 (IM7)	BD Biosciences	Cat# 563736, RRID:AB_2738395
Anti-mouse CD44 AF700 (IM7)	Thermo Fisher Scientific	Cat# 56-0441-82 RRID:AB_494011
Anti-Mouse CD69 PE-Cy7 (H1.2F3)	BD Biosciences	Cat# 552879, RRID:AB_394508
Anti-Mouse CD69 BV605 (H1.2F3)	BD Biosciences	Cat# 104529, RRID:AB_11203710
Anti-mouse CD103 BV510 (M290)	BD Biosciences	Cat# 563087, RRID:AB_2721775
Anti-mouse P2X7 PE (1F11)	BD Biosciences	Cat# 565345, RRID:AB_2739198
Anti-mouse P2X7R APC (1F11)	BioLegend	Cat# 148706, RRID:AB_2650954
Anti-mouse CD279 (PD-1) (RMP1-130)	BioLegend	Cat# 109119, RRID:AB_2566640
Anti-Mouse CD279 (PD-1) (RMP1-130)	BD Biosciences	Cat# 748264, RRID:AB_2872692
Anti-Mouse CD39 PerCP-eFluor 710 (24DMS1)	Thermo Fisher Scientific	Cat# 46-0391-82, RRID:AB_10717953
Anti-Mouse CD223 (LAG-3) PE/Dazzle 594 (C9B7W)	BioLegend	Cat# 125224, RRID:AB_2572082
Anti-Mouse CD366 (Tim-3) BV421 (RMT3-23)	BioLegend	Cat# 119723, RRID:AB_2616908
Anti-Mouse TCF1/7 PE (C63/D9)	Cell Signaling Technologies	Cat# 14456S RRID: AB_10828102
Anti-Mouse TOX eFluor 660 (TXRX10)	Thermo Fisher Scientific	Cat# 50-6502-82 RRID: AB_2574265
Anti-Mouse Ki-67 FITC (SolA15)	Thermo Fisher Scientific	Cat# 11-5698-82 RRID: AB_11151330
Anti-Mouse IFN-γ PE-Cy7 (XMG1.2)	BioLegend	Cat# 505826 RRID: AB_2295770
Anti-Mouse Granzyme B PE (GB11)	Thermo Fisher Scientific	Cat# 12-8899-41 RRID: AB_1659718
Annexin V APC	BD Biosciences	Cat# 550475 RRID: AB_2868885
Ghost Dye Red 780 Viability Dye	Tonbo Biosciences	Cat # 13-0865-T100
MitoTracker Green FM	Thermo Fisher Scientific	Cat # M7514
MitoSOX Red Mitochondrial Superoxide Indicator	Thermo Fisher Scientific	Cat # M36008
Tetramethylrhodamine, Ethyl Ester, Perchlorate (TMRE)	Thermo Fisher Scientific	Cat # T669
CellTrace Far Red Cell Proliferation Kit	Thermo Fisher Scientific	Cat# C34564
InCucyte Caspase 3/7 Dye for Apoptosis	Sartorius	Cat# 4440
InVivoMAb anti-mouse CD3ε (145-2C11)	BioXCell	Cat# BE0001-1, RRID:AB_1107634
InVivoMAb anti-mouse CD28 (37.51)	BioXCell	Cat# BE0015-1, RRID:AB_1107624
Chemicals, peptides, and recombinant proteins		
Collagenase, Type 1	Worthington	Cat# LS004197

REAGENT or RESOURCE	SOURCE	IDENTIFIER
Dithioerythritol	EMD Millipore	Cat# 233152-5GM
RPMI 1640	Corning	Cat# 10-040-CV
HBSS 10x	Corning	Cat# 20-021-CV
Fetal Bovine Serum	Atlas Biologicals	Cat# FS-0500-AD
L-Glutamine, 100x, Liquid	Corning	Cat# 25-005-CI
Penicillin/Streptomycin	Gibco	Cat# 15070063
DMEM	Gibco	Cat# 11995065
A-438079	Abcam	Cat# ab120413
Human recombinant IL-2	Peprotech	Cat# 200-02
Mouse recombinant IL-12	R&D Systems	Cat# 419-ML-050/CF
Human recombinant IL-12	R&D Systems	Cat# 219-IL-005/CF
2'(3')-O-(4-Benzoylbenzoyl) adenosine 5'-triphosphate triethylammonium salt (Bz-ATP)	Sigma-Aldrich	Cat# B6396-25MG
XF Base Medium Minimal DMEM	Agilent Technologies	Cat# 102353-100
Critical commercial assays		
Naïve CD8a+ T cell Isolation Kit, Mouse	Miltenyi Biotec	Cat# 130-096-543
BD Cytofix/Cytoperm Solution Kit	BD Biosciences	Cat#554714
FoxP3/Transcription Factor Staining Buffer Set	Tombo Bioscience	Cat# TNB-0607-KIT
Naive CD8a+ T cell Isolation Kit, Human	Stem Cell Technologies	Cat# 19258
Seahorse XF Cell Mito Stress Test Kit	Agilent Technologies	Cat# 103015-100
QiaShredder Columns	Qiagen	Cat# 79654
RNeasy Plus Mini Kit	Qiagen	Cat# 74134
SuperScript III First-Strand Synthesis SuperMix	Invitrogen	Cat# 11752050
SYBR Green PCR Master Mix	Thermo Fisher Scientific	Cat# 4309155
Experimental models: Cell lines		
B16.OVA Murine Melanoma	Dr. M. Mescher, University of Minnesota	N/A
B16.gp33 Murine Melanoma	Dr. A. Goldrath, University of San Diego	N/A
Experimental models: Organisms/strains		
Mouse: B6.SJL-Ptprc^{a}Pepc^{b}/BoyCrCrl (B6-CD45.1)	NCI Charles River	Cat# CRL:564, RRID:IMSR_CRL:564
Mouse: C57BL/6NCrl (B6-CD45.2)	NCI Charles River	Cat# CRL:027, RRID:IMSR_CRL:027
Mouse: P14	Dr. R. Ahmed, Emory University	N/A
Mouse: OT-I	Dr. K. Hogquist, University of Minnesota	N/A
Mouse: B6.129P2-P2rx7^{tm1Gab}/J (*P2rx7*$^{-/-}$)	Jackson Labs	Stock# 005576
Oligonucleotides		
hP2rx7 Forward Primer: 5'- TGT GTC CCG AGT ATC CCA CC -3'	Integrated Data Technologies	N/A

REAGENT or RESOURCE	SOURCE	IDENTIFIER
hP2rx7 Reverse Primer 5'- GGC ACT GTT CAA GAG AGC AG -3'	Integrated Data Technologies	N/A
hGUSB Forward Primer 5'- GTC TGC GGC ATT TTG TCG -3'	Integrated Data Technologies	N/A
hGUSB Reverse Primer 5'- CAC ACG ATG GCA TAG GAA TGG -3'	Integrated Data Technologies	N/A
Software and algorithms		
GraphPad Prism v9.2.0	GraphPad Software	RRID:SCR_002798
FlowJo v10.8	BD Biosciences	RRID:SCR_008520
BD FACSDiva	BD Biosciences	RRID:SCR_001456
Seahorse Wave Desktop Software	Agilent Technologies	RRID: SCR_014526